Accelerated hydrological cycle over the Sanjiangyuan region induces more streamflow extremes at different global warming levels

Peng Ji[1,2], Xing Yuan[3*], Feng Ma[3], Ming Pan[4]

[1]Key Laboratory of Regional Climate-Environment for Temperate East Asia, Institute of Atmospheric Physics, Chinese Academy of Sciences, Beijing 100029, China

[2]College of Earth and Planetary Sciences, University of Chinese Academy of Sciences, Beijing 1000493, China

[3]School of Hydrology and Water Resources, Nanjing University of Information Science and Technology, Nanjing 210044, China

[4]Department of Civil and Environmental Engineering, Princeton University, Princeton, New Jersey, USA

Correspondence to: Xing Yuan (xyuan@nuist.edu.cn)

Abstract. Serving source water for the Yellow, Yangtze and Lancang-Mekong rivers, the Sanjiangyuan region concerns 700 million people over its downstream areas. Recent research suggests that the Sanjiangyuan region will become wetter in a warming future, but future changes of streamflow extremes remain unclear due to the complex hydrological processes over high-land areas and limited knowledge of the influences of land cover change and CO_2 physiological forcing. Based on high resolution land surface modeling during 1979~2100 driven by the climate and ecological projections from 11 newly released Coupled Model Intercomparison Project Phase 6 (CMIP6) climate models, we show that different accelerating rates of precipitation and evapotranspiration at 1.5°C global warming level induce 55% more dry extremes over Yellow river and 138% more wet extremes over Yangtze river headwaters compared with the reference period (1985~2014). An additional 0.5°C warming leads to a further nonlinear and more significant increase for both dry extremes over Yellow river (22%) and wet extremes over Yangtze river (64%). The combined role of CO_2 physiological forcing and vegetation greening, which used to be neglected in hydrological projections, is found to alleviate dry extremes at 1.5 and 2.0°C warming levels but to intensify dry extremes at 3.0°C warming level. Moreover, vegetation greening contributes half of the differences between 1.5 and 3.0°C warming levels. This study emphasizes the importance of ecological processes in determining future changes in streamflow extremes, and suggests a "dry gets drier, wet gets wetter" condition over the warming headwaters.

Keywords Terrestrial hydrological cycle, streamflow extremes, global warming levels,

38 CMIP6, Sanjiangyuan, land cover change

1 Introduction

Global temperature has increased at a rate of 0.17°C/decade since 1970, contrary to the cooling trend over the past 8000 years (Marcott et al., 2013). The temperature measurements suggest that 2015-2019 is the warmest five years and 2010-2019 is also the warmest decade since 1850 (WMO, 2020). To mitigate the impact of this unprecedented warming on the global environment and human society, 195 nations adopted the Paris Agreement which decides to "hold the increase in the global average temperature to well below 2°C above pre-industrial levels and pursing efforts to limit the temperature increase to 1.5°C".

The response of regional and global terrestrial hydrological processes (e.g., streamflow and its extremes) to different global warming levels has been investigated by numerous studies in recent years (Döll et al., 2018; Hoegh-Guldberg et al., 2018; Marx et al., 2018; Mohammed et al., 2017; Thober et al., 2018; Xu et al., 2019; Zhang et al., 2016). In addition to climate change, recent works reveal the importance of the ecological factors (e.g., the CO_2 physiological forcing and land cover change), which are often unaccounted for in hydrological modeling works, in modulating the streamflow and its extremes. For example, the increasing CO_2 concentration is found to alleviate the decreasing trend of streamflow in the future at global scale through decreasing the stomatal conductance and vegetation transpiration (known as the CO_2 physiological forcing) (Fowler et al., 2019; Wiltshire et al., 2013; Yang et al., 2019; Zhu et al., 2012). Contrary to the CO_2 physiological forcing, the vegetation greening in a warming climate is found to play a significant role in exacerbating hydrological

drought, as it enhances transpiration and dries up the land (Yuan et al., 2018b). However, the relative contributions of CO_2 physiological forcing and vegetation greening to the changes in terrestrial hydrology especially the streamflow extremes are still unknown, and whether their combined impact differs among different warming levels needs to be investigated.

Hosting the headwaters of the Yellow river, the Yangtze river and the Lancang-Mekong river, the Sanjiangyuan region is known as the "Asian Water Tower" and concerns 700 million people over its downstream areas. Changes of streamflow and its extremes over the Sanjiangyuan region not only influence the local ecosystems, environment and water resources, but also the security of food, energy, and water over the downstream areas. Both the regional climate and ecosystems show significant changes over the Sanjiangyuan region due to global warming (Bibi et al., 2018; Kuang and Jiao, 2016; Liang et al., 2013; Yang et al., 2013; Zhu et al., 2016). Historical changes of climate and ecology (e.g. land cover) are found to cause significant reduction in mean and high flows over the Yellow River headwaters during 1979-2005, which potentially increases drought risk over its downstream areas (Ji and Yuan, 2018). And the CO_2 physiological forcing is revealed to cause equally large changes in regional flood extremes as the precipitation over the Yangtze and Mekong rivers (Fowler et al., 2019). Thus the Sanjiangyuan region is a sound region to investigate the role of climate change and ecological change (e.g., land cover change and CO_2 physiological forcing) in influencing the streamflow and its extremes (Cuo et al., 2014; Ji and Yuan, 2018; Zhu et al., 2013). Recent research suggests that the

Sanjiangyuan region will become warmer and wetter in the future, and extreme precipitation will also increase at the 1.5°C global warming level and further intensify with a 0.5°C additional warming (Li et al., 2018; Zhao et al., 2019). However, how the streamflow extremes would respond to the 1.5°C warming, what an additional 0.5°C or even greater warming would cause, and how much contributions do the ecological factors (e.g., CO_2 physiological forcing and land cover change) have, are still unknown. Solving the above issues is essential for assessing the climate and ecological impact on this vital headwaters region.

In this study, we investigated the future changes in the streamflow extremes over the Sanjiangyuan region from an integrated eco-hydrological perspective by taking CO_2 physiological forcing and land cover change into consideration. The combined impacts of the above two ecological factors at different global warming levels were also quantified and compared with the impact of climate change. The results will help understand the role of ecological factors in future terrestrial hydrological changes over the headwater regions like the Sanjiangyuan, and provide guidance and support for the stakeholders to make relevant decisions and plans.

2 Data and methods

2.1 Study domain and observational data

The Sanjiangyuan region is located at the eastern part of the Tibetan Plateau (Figure 1a), with the total area and mean elevation being 3.61×10^5 km^2 and 5000 m respectively. It plays a critical role in providing freshwater, by contributing 35%, 20% and 8% to the total annual streamflow of the Yellow, Yangtze and Lancang-Mekong

105 rivers (Li et al., 2017; Liang et al., 2013). The source regions of Yellow, Yangtze and
106 Lancang-Mekong rivers account for 46%, 44% and 10% of the total area of the
107 Sanjiangyuan individually, and the Yellow river source region has a warmer climate
108 and sparser snow cover than the Yangtze river source region.

109 Monthly streamflow observations from the Tangnaihai (TNH) and the Zhimenda
110 (ZMD) hydrological stations (Figure 1a), which were provided by the local authorities,
111 were used to evaluate the streamflow simulations. Data periods are 1979-2011 and
112 1980-2008 for the Tangnaihai and Zhimenda stations individually. Estimations of
113 monthly terrestrial water storage change and its uncertainty during 2003-2014 were
114 provided by the Jet Propulsion Laboratory (JPL), which used the mass concentration
115 blocks (mascons) basis functions to fit the Gravity Recovery and Climate Experiment
116 (GRACE) satellite's inter-satellite ranging observations (Watkins et al., 2015). The
117 Model Tree Ensemble evapotranspiration (MTE_ET; Jung et al., 2009) and the Global
118 Land Evaporation Amsterdam Model evapotranspiration (GLEAM_ET) version 3.3a
119 (Martens et al., 2017) were used to evaluate the ET simulation.

120 **2.2 CMIP6 Data**

121 Here, 19 Coupled Model Intercomparison Project phase 6 (CMIP6, Eyring et al.,
122 2016) models which provide precipitation, near-surface temperature, specific
123 humidity, 10-m wind speed, surface downward shortwave and longwave radiations at
124 daily timescale were first selected for evaluation. Then, models were chosen for the
125 analysis when the simulated meteorological forcings (e.g., precipitation, temperature,
126 humidity, and shortwave radiation) averaged over the Sanjiangyuan region have the

same trend signs as the observations during 1979-2014. Table 1 shows the 11 CMIP6 models that were finally chosen in this study. For the future projection (2015-2100), we chose two Shared Socioeconomic Pathways (SSP) experiments: SSP585 and SSP245. SSP585 combines the fossil-fueled development socioeconomic pathway and 8.5W/m^2 forcing pathway (RCP8.5), while SSP245 combines the moderate development socioeconomic pathway and 4.5 W/m^2 forcing pathway (RCP4.5) (O'Neill et al., 2016). Land cover change is quantified by leaf area index (LAI) as there is no significant transition between different vegetation types (not shown) according to the Land-use Harmonization 2 (LUH2) dataset (https://esgf-node.llnl.gov/search/input4mips/). For the CNRM-CM6-1, FGOALS-g3 and CESM2, the ensemble mean of LAI simulations from the other 8 CMIP6 models was used because CNRM-CM6-1 and FGOALS-g3 do not provide dynamic LAI while the CESM2 simulates an abnormally large LAI over the Sanjiangyuan region. To avoid systematic bias in meteorological forcing, the trend-preserved bias correction method suggested by ISI-MIP (Hempel et al., 2013), was applied to the CMIP6 model simulations at monthly scale. The China Meteorological Forcing Dataset (CMFD) was taken as meteorological observation (He et al., 2020). For each month, temperature bias in CMIP6 simulations during 1979-2014 was directly deducted. Future temperature simulations in SSP245 and SSP585 experiments were also adjusted according to the historical bias. Other variables were corrected by using a multiplicative factor, which was calculated by using observations to divide simulation during 1979-2014. In addition, monthly leaf area index was also adjusted

149 to be consistent with satellite observation using the same method as temperature. All
150 variables were first interpolated to the 10 km resolution over the Sanjiangyuan region
151 and the bias correction was performed for each CMIP6 model at each grid. After bias
152 correction, absolute changes of temperature and leaf area index, and relative changes
153 of other variables were preserved at monthly time scale (Hempel et al., 2013). Then,
154 the adjusted CMIP6 daily meteorological forcings were disaggregated into hourly
155 using the diurnal cycle ratios from the China Meteorological Forcing Dataset.

156 The historical CO_2 concentration used here is the same as the CMIP6 historical
157 experiment (Meinshausen et al., 2017), while future CO_2 concentration in SSP245 and
158 SSP585 scenarios came from simulations of a reduced-complexity carbon-cycle
159 model MAGICC7.0 (Meinshausen et al., 2020).

160 **2.3 Experimental design**

161 The land surface model used in this study is the Conjunctive Surface-Subsurface
162 Process model version 2 (CSSPv2), which has been proved to simulate the energy and
163 water processes over the Sanjiangyuan region well (Yuan et al., 2018a). Figure 2
164 shows the structure and main ecohydrological processes in CSSPv2. The CSSPv2 is
165 rooted in the Common Land Model (CoLM; Dai et al., 2003) with some
166 improvements at hydrological processes. CSSPv2 has a volume-averaged soil
167 moisture transport (VAST) model, which solves the quasi-three dimensional
168 transportation of the soil water and explicitly considers the variability of moisture flux
169 due to subgrid topographic variations (Choi et al., 2007). Moreover, the Variable
170 Infiltration Capacity runoff scheme (Liang et al., 1994), and the hydrological

properties of soil organic matters were incorporated into the CSSPv2 by Yuan et al. (2018a), to improve its performance in simulating the terrestrial hydrology over the Sanjiangyuan region. Similar to CoLM and Community Land Model (Oleson et al., 2013), vegetation transpiration in CSSPv2 is based on Monin-Obukhov similarity theory, and the transpiration rate is constrained by leaf boundary layer and stomatal conductances. Parameterization of the stomatal conductance (g_s) in CSSPv2 is

$$g_s = m \frac{A_n}{P_{CO_2} / P_{atm}} h_s + b\beta_t \quad (1)$$

where the m is a plant functional type dependent parameter, A_n is leaf net photosynthesis ($\mu mol\ CO_2\ m^{-2}\ s^{-1}$), P_{CO_2} is the CO_2 partial pressure at the leaf surface (Pa), P_{atm} is the atmospheric pressure (Pa), h_s is the lead surface humidity, b is the minimum stomatal conductance ($\mu mol\ m^{-2}\ s^{-1}$), while β_t is the soil water stress function. Generally, the stomatal conductance decreases with the increasing of CO_2 concentration.

First, bias-corrected meteorological forcings from CMIP6 historical experiment were used to drive the CSSPv2 model (CMIP6_His/CSSPv2). All simulations were conducted for two cycles during 1979-2014 at half-hourly time step and 10 km spatial resolution, with the first cycle serving as the spin-up. Correlation coefficient (CC) and root mean squared error (RMSE) were calculated for validating the simulated monthly streamflow, annual evapotranspiration and monthly terrestrial water storage. The King-Gupta efficiency (KGE; Gupta et al., 2009), which is widely used in streamflow evaluations, was also calculated. Above metrics were calculated as follows:

$$CC = \frac{\sum_{i=1}^{n}(x_i - \bar{x})(y_i - \bar{y})}{\sqrt{\sum_{i=1}^{n}(x_i - \bar{x})^2 \sum_{i=1}^{n}(y_i - \bar{y})^2}} \quad (2)$$

$$RMSE = \sqrt{\frac{\sum_{i=1}^{n}(x_i - y_i)^2}{n}} \quad (3)$$

$$KGE = 1 - \sqrt{(1 - CC)^2 + (1 - \frac{\sigma_x}{\sigma_y})^2 + (1 - \frac{\bar{x}}{\bar{y}})^2} \quad (4)$$

where x_i and y_i are observed and simulated variables in a specific month/year i individually, and $\bar{x}$ and $\bar{y}$ are the corresponding monthly/annual means during the evaluation period n. The σ_x and σ_y are standard deviations for observed and simulated variables respectively. The correlation coefficient represents the correlation between simulation and observation, while RMSE means simulated error. The KGE ranges from negative infinity to 1, and model simulations can be regard as satisfactory when the KGE is larger than 0.5 (Moriasi et al., 2007).

Second, bias-corrected meteorological forcings in SSP245 and SSP585 were used to drive CSSPv2 during 2015-2100 with dynamic LAI and CO_2 concentration (CMIP6_SSP/CSSPv2). Initial conditions of CMIP6_SSP/CSSPv2 came from the last year in CMIP6_His/CSSPv2.

Then, the second step was repeated twice by fixing the monthly LAI (CMIP6_SSP/CSSPv2_FixLAI) and mean CO_2 concentration (CMIP6_SSP/CSSPv2_FixCO2) at 2014 level. The difference between CMIP6_SSP/CSSPv2 and CMIP6_SSP/CSSPv2_FixLAI is regarded as the net effect of land cover change, and the difference between CMIP6_SSP/CSSPv2 and

CMIP6_SSP/CSSPv2_FixCO2 is regarded as the net effect of CO_2 physiological forcing.

2.4 Warming level determination

A widely used time-sampling method was adopted to determine the periods of different global warming levels (Chen et al., 2017; Döll et al., 2018; Marx et al., 2018; Mohammed et al., 2017; Thober et al., 2018). According to the HadCRUT4 dataset (Morice et al., 2012), the global mean surface temperature has increased by 0.66°C from the pre-industrial era (1850-1900) to the reference period defined as 1985-2014. Then, starting from 2015, 30-years running mean global temperatures were compared to those of the 1985-2014 period for each GCM simulation. And the 1.5°C/2.0°C/3.0°C warming period is defined as the 30-years period when the 0.84°C/1.34°C/2.34°C global warming, compared with the reference period (1985-2014), is first reached. The median years of identified 30-year periods, referred as "crossing years", are shown in Table 2.

2.5 Definition of dry and wet extremes and robustness assessment

In this research, the standardized streamflow index (SSI) was used to define dry and wet extremes (Vicente-Serrano et al., 2012; Yuan et al., 2017). The July-August-September (JAS) mean streamflow for each year of the reference period was first collected and used to fit a gamma distribution:

$$f(x,\beta,\alpha)=\frac{\beta^{\alpha}}{\Gamma(\alpha)}x^{\alpha-1}e^{-\beta x} \tag{5}$$

where x means streamflow, while α and β are parameters. Then the fitted distribution was used to standardize the JAS mean streamflow in each year (i) during

both the reference and projection periods as:

$$SSI_i = Z^{-1}(F(x_i))$$
$$F(x_i) = \int_0^{x_i} f(x, \beta, \alpha)\, dx \quad (6)$$

where Z^{-1} means the inverse cumulative distribution function of the normal distribution, while $F(x)$ is the cumulative distribution function of the gamma distribution. Here, dry and wet extremes were defined as SSIs smaller than -1.28 (a probability of 10%) and larger than 1.28 respectively.

The relative changes in frequency of dry/wet extremes between the reference period and different warming periods were first calculated for each GCM under each SSP scenario, and the ensemble means were then determined for each warming level. To quantify the uncertainty, the above calculations were repeated by using the bootstrap 10,000 times, and 11 GCMs were resampled with replacement during each bootstrap (Christopher et al., 2018). The 5% and 95% percentiles of the total 10,000 estimations were finally taken as the 5~95% uncertainty ranges.

3 Results

3.1 Terrestrial hydrological changes at different warming levels

As shown in Figures 1b-1e, observations (pink lines) show that the annual temperature, precipitation and growing season LAI increase at the rates of 0.63°C/decade (p=0), 16.9 mm/decade (p=0.02), and 0.02 m^2/m^2/decade (p=0.001) during 1979-2014 respectively. The ensemble means of CMIP6 simulations (black lines) can generally capture the historical increasing trends of temperature (0.30 °C/decade, p=0), precipitation (7.1 mm/decade, p=0) and growing season LAI (0.029 m^2/m^2/decade, p=0), although the trends for precipitation and temperature are

underestimated. In 2015-2100, the SSP245 scenario (blue lines) shows continued warming, wetting and greening trends, and the trends are larger in the SSP585 scenario (red lines). The CO_2 concentration also keeps increasing during 2015-2100 and reaches to 600 ppm and 1150 ppm in 2100 for the SSP245 and SSP585 scenarios respectively. Although the SSP585 scenario reaches the same warming levels earlier than the SSP245 scenario (Table 2), there is no significant difference between them in the meteorological variables during the same warming period (not shown). Thus, we do not distinguish SSP245 and SSP585 scenarios at the same warming level in the following analysis.

Figure 3 and Table 3 show the evaluation of model simulation. Driven by observed meteorological and ecological forcings, the CMFD/CSSPv2 simulates monthly streamflow over the Yellow and Yangtze river headwaters quite well. The Kling-Gupta efficiencies of CMFD/CSSPv2 simulated monthly streamflow are 0.94 and 0.91 over Tangnaihai (TNH) and Zhimenda (ZMD) stations, respectively. The simulated monthly Terrestrial Water Storage Anomaly (TWSA) during 2003-2014 in CMFD/CSSPv2 also agrees with the GRACE satellite observation and captures the increasing trend. For the interannual variations of evapotranspiration, CMFD/CSSPv2 is consistent with the ensemble mean of the GLEAM_ET and MTE_ET products, and the correlation coefficient and root mean squared error (RMSE) during 1982-2011 are 0.87 ($p<0.01$) and 14 mm/year respectively. This suggests the good performance of the CSSPv2 in simulating the hydrological processes over the Sanjiangyuan region. Although meteorological and ecological outputs from CMIP6 models have coarse

277 resolutions (~100 km), the land surface simulation driven by bias corrected CMIP6
278 results (CMIP6_His/CSSPv2) also captures the terrestrial hydrological variations
279 reasonably well. The Kling-Gupta efficiency of the ensemble mean streamflow
280 simulation reaches up to 0.71~0.81, and the ensemble mean monthly Terrestrial Water
281 Storage Anomaly (TWSA) and annual evapotranspiration generally agree with
282 observations and other reference data (Figures 3c-3d).

283 Figure 4 shows relative changes of terrestrial hydrological variables over the
284 Sanjiangyuan region at different warming levels. The ensemble mean of the increase
285 in annual precipitation is 5% at 1.5°C warming level, and additional 0.5°C and 1.5°C
286 warming will further increase the wetting trends to 7% and 13% respectively. Annual
287 evapotranspiration experiences significant increases at all warming levels, and the
288 ensemble mean increases are 4%, 7% and 13% at 1.5, 2.0 and 3.0°C warming levels
289 respectively. The ratio of transpiration to evapotranspiration also increases
290 significantly, indicating that vegetation transpiration increases much larger than the
291 soil evaporation and canopy evaporation. Although annual total runoff has larger
292 relative changes than evapotranspiration (6%, 9% and 14% at 1.5, 2.0 and 3.0°C
293 warming levels respectively), the uncertainty is large as only 75% of the models show
294 positive signals, which may be caused by large uncertain changes during summer and
295 autumn seasons. The terrestrial water storage (TWS) which includes foliage water,
296 surface water, soil moisture and groundwater, shows slightly decreasing trend at
297 annual scale, suggesting that the increasing precipitation in the future becomes extra
298 evapotranspiration and runoff instead of recharging the local water storage. The

accelerated terrestrial hydrological cycle also exists at seasonal scale, as the seasonal changes are consistent with the annual ones.

3.2 Changes in streamflow extremes at different warming levels

Although the intensified terrestrial hydrology induces more streamflow over the headwater region of Yellow river during winter and spring months, streamflow does not increase and even decreases during the flood season (July-September; Figure 5a). Figure 5b shows the changes of streamflow dry extremes over the Yellow river source region at different warming levels, with the error bars showing estimated uncertainties. The frequency of streamflow dry extremes over the Yellow river is found to increase by 55% at 1.5°C warming level (Figure 5b), but the uncertainty is larger than the ensemble mean. However, the dry extreme frequency will further increase to 77% and 125% at the 2.0 and 3.0°C warming levels and the results become significant (Figure 5b). No statistically significant changes are found for the wet extremes at all warming levels over the Yellow River headwater region, as the uncertainty ranges are larger than the ensemble means.

Over the Yangtze river headwater region, streamflow increases in all months at different warming levels (Figure 5c). The frequency of wet extremes increases significantly by 138%, 202% and 232% at 1.5, 2.0 and 3.0°C warming levels (Figure 5d), suggesting a higher risk of flooding. Although the frequency of dry extremes also tends to decrease significantly by 35%, 44%, 34% at the three warming levels, the changes are much smaller than those of the wet extremes. Moreover, contributions from climate change and ecological change are both smaller than the uncertainty

ranges (not shown), suggesting that their impacts on the changes of dry extremes over the Yangtze river headwater region are not distinguishable. Thus, we mainly focus on the dry extremes over the Yellow river and the wet extremes over the Yangtze river in the following analysis.

Different changes of streamflow extremes over the Yellow and Yangtze rivers can be interpreted from different accelerating rates of precipitation and evapotranspiration. Figure 6 shows probability density functions (PDFs) of precipitation, evapotranspiration and their difference (P-ET, i.e. residual water for runoff generation) during the flood season. Over the Yellow river, PDFs of precipitation and evapotranspiration both shift to the right against the reference period, except for the precipitation at 1.5°C warming level. However, the increasing trend of evapotranspiration is stronger than that of precipitation, leading to a left shift for the PDF of P-ET. Moreover, increased variations of precipitation and evapotranspiration, as indicated by the increased spread of their PDFs, also lead to a larger spread of PDFs of P-ET. The above two factors together induce a heavier left tail in the PDF of P-ET for the warming future than the reference period (Figure 6e). The probability of P-ET<80mm increases from 0.1 during historical period to 0.11, 0.13 and 0.16 at 1.5, 2.0 and 3.0°C warming levels individually. This indicates a higher probability of less water left for runoff generation at different warming levels, given little changes in TWS (section 3.1). Moreover, Figure 6e also shows little change in the right tails of the PDF of P-ET as probability for P-ET>130mm stays around 0.1 at different warming levels, suggesting little change to the probability of high residual water. This

is consistent with the insignificant wet extreme change over the Yellow river. Over the Yangtze river, however, intensified precipitation is much larger than the increased evapotranspiration, leading to a systematic rightward shift of the PDF of P-ET (Figures 6b, 6d and 6f). Thus both the dry and wet extremes show significant changes over the Yangtze river.

3.3 Influences of land cover change and CO_2 physiological forcing

Figures 7a-7b show the changes of streamflow extremes (compared with the reference period) induced by climate and ecological factors. Although the contribution from climate change (red bars in Figures 7a-7b) is greater than the ecological factors (blue and cyan bars in in Figures 7a-7b), influences of CO_2 physiological forcing and land cover change are nontrivial. The CO_2 physiological forcing tends to alleviate dry extremes (or increase wet extremes), while land cover change plays a contrary role. Over the Yellow river, the combined impact of the two ecological factors (sum of blue and cyan bars) reduces the increasing trend of dry extremes caused by climate change (red bars) by 18~22% at 1.5 and 2.0 °C warming levels, while intensifies the dry extremes by 9% at 3.0°C warming level. This can be interpreted from their contributions to the evapotranspiration, as enhancement effect of the increased LAI on ET is weaker than the suppression effect of CO_2 physiological forcing at 1.5 and 2.0°C warming levels, while stronger at 3.0°C warming level (not shown). Over the Yangtze river, similarly, combined effect of land cover and CO_2 physiological forcing increases the wet extremes by 9% at 1.5°C warming level while decreases the wet extremes by 12% at 3.0°C warming level.

In addition, Figures 7c and 7d show that the combined impact of CO_2 physiological forcing and land cover change also influences the differences between different warming levels. Over the Yellow river, climate change increases dry extremes by 26% from 1.5 to 2.0°C warming level, and by 40% from 1.5 and 3.0°C warming level (red bars in Figure 7c). After considering the two ecological factors (pink bars in Figure 7c), above two values change to 22% and 70% respectively, and the difference between 1.5 and 3.0°C warming levels becomes significant. For the wet extreme over the Yangtze river (Figure 7d), the climate change induced difference between 1.5 and 2.0°C warming levels is decreased by 16% after accounting for the two ecological factors. And this decrease reaches up to 49% for the difference between 1.5 and 3.0°C warming levels. We also compared the scenarios when CO_2 physiological forcing and land cover change are combined with climate change individually (blue and cyan bars in Figures 7c-d), and the results show the land cover change dominates their combined influences on the difference between different warming levels.

4 Conclusions and Discussion

This study investigates changes of streamflow extremes over the Sanjiangyuan region at different global warming levels through high-resolution land surface modeling driven by CMIP6 climate simulations. The terrestrial hydrological cycle under global warming of 1.5°C is found to accelerate by 4~6% compared with the reference period of 1985-2014, according to the relative changes of precipitation, evapotranspiration and total runoff. The terrestrial water storage, however, shows a

387 slight but significant decreasing trend as increased evapotranspiration and runoff are
388 larger than the increased precipitation. This decreasing trend of terrestrial water
389 storage in the warming future is also found in six major basins in China (Jia et al.,
390 2020). Although streamflow changes during the flood season has a large uncertainty,
391 the frequency of wet extremes over the Yangtze river will increase significantly by
392 138% and that of dry extremes over the Yellow river will increase by 55% compared
393 with that during 1985~2014. With an additional 0.5°C warming, the frequency of dry
394 and wet extremes will increase further by 22~64%. If the global warming is not
395 adequately managed (e.g., to reach 3.0°C), wet extremes over the Yangtze river and
396 dry extremes over the Yellow river will increase by 232% and 125%. The changes
397 from 1.5 to 2.0 and 3.0°C are nonlinear compared with that from reference period to
398 1.5°C, which are also found for some fixed-threshold climate indices over the Europe
399 (Dosio and Fischer, 2018). It is necessary to cap the global warming at 2°C or even
400 lower level, to reduce the risk of wet and dry extremes over the Yangtze and Yellow
401 rivers.

402 This study also shows the nontrivial contributions from land cover change and
403 CO_2 physiological forcing to the extreme streamflow changes especially at 2.0 and
404 3.0°C warming levels. The CO_2 physiological forcing is found to increase streamflow
405 and reduce the dry extreme frequency by 14~24%, which is consistent with previous
406 findings that CO_2 physiological forcing would increase available water and reduce
407 water stress at the end of this century (Wiltshire et al., 2013). However, our results
408 further show that the drying effect of increasing LAI on streamflow will exceed the

409 wetting effect of CO_2 physiological forcing at 3.0°C warming level (during
410 2048~2075) over the Sanjiangyuan region, making a reversion in the combined
411 impacts of CO_2 physiological forcing and land cover. Thus it is vital to consider the
412 impact of land cover change in the projection of future water stress especially at high
413 warming scenarios.

414 Moreover, about 43~52% of the extreme streamflow changes between 1.5 and
415 3.0°C warming levels are attributed to the increased LAI. Considering the LAI
416 projections from different CMIP6 models are induced by the climate change, it can be
417 inferred that the indirect influence of climate change (e.g., through land cover change)
418 has the same and even larger importance on the changes of streamflow extremes
419 between 1.5 and 3.0°C or even higher warming levels, compared with the direct
420 influence (e.g., through precipitation and evapotranspiration). Thus, it is vital to
421 investigate hydrological and its extremes changes among different warming levels
422 from an eco-hydrological perspective instead of focusing on climate change alone.

423 Although we used 11 CMIP6 models combined with two SSP scenarios to reduce
424 the uncertainty of future projections caused by GCMs, using a single land surface
425 model may result in uncertainties (Marx et al., 2018). However, considering the good
426 performance of the CSSPv2 land surface model over the Sanjiangyuan region and the
427 dominant role of GCMs' uncertainty (Zhao et al., 2019; Samaniego et al., 2017),
428 uncertainty from the CSSPv2 model should have limited influence on the robustness
429 of the result.

430

Acknowledgments We thank the World Climate Research Programme's Working Group on Couple modelling for providing CMIP6 data (https://esgf-node.llnl.gov). This work was supported by National Key R&D Program of China (2018YFA0606002) and National Natural Science Foundation of China (41875105, 91547103), and the Startup Foundation for Introducing Talent of NUIST.

Competing interests

The authors declare that they have no conflict of interest.

References

Bibi, S., Wang, L., Li, X., Zhou, J., Chen, D., and Yao, T.: Climatic and associated cryospheric, biospheric, and hydrological changes on the Tibetan Plateau: a review, Int. J. Climatol., 38, e1-e17, https://doi.org/10.1002/joc.5411, 2018.

Chen, J., Gao, C., Zeng, X., Xiong, M., Wang, Y., Jing, C. Krysanova, V., Huang, J., Zhao, N., and Su, B.: Assessing changes of river discharge under global warming of 1.5° C and 2° C in the upper reaches of the Yangtze River Basin: Approach by using multiple-GCMs and hydrological models, Quatern. Int., 453, 1 – 11, http://dx.doi.org/10.1016/j.quaint.2017.01.017, 2017.

Cuo, L., Zhang, Y., Zhu, F., and Liang, L.: Characteristics and changes of streamflow on the Tibetan Plateau: A review, J. Hydrol.-Reg. Stud., 2, 49 – 68, https://doi.org/10.1016/j.ejrh.2014.08.004, 2014.

Dai, Y. J., Zeng, X. B., Dickinson, R. E., Baker, I., Bonan, G. B., Bosilovich, M. G., Denning, A. S., Dirmeyer, P. A., Houser, P. R., Niu, G. Y., Oleson, K. W., Schlosser, C. A., and Yang, Z. L.: The Common Land Model. B. Am. Meteorol. Soc., 84, 1013 – 1024, https://doi.org/10.1175/BAMS-84-8-1013, 2003.

Döll, P., Trautmann, T., Gerten, D., Schmied, H. M., Ostberg, S., Saaed, F., and Schleussner, C.: Risks for the global freshwater system at 1.5° C and 2° C global warming. Environ. Res. Lett., 13, 044038, https://doi.org/10.1088/1748-9326/aab792, 2018.

Dosio, A., and Fischer, E. M.: Will half a degree make a difference? Robust projections of indices of mean and extreme climate in Europe under 1.5° C, 2°

462 C, and 3 ° C global warming, Geophys. Res. Lett., 45.
463 https://doi.org/10.1002/2017GL076222, 2018.
464 Eyring, V., Bony, S., Meehl, G. A., Senior, C. A., Stevens, B., Stouffer, R. J., and
465 Taylor, K. E.: Overview of the Coupled Model Intercomparison Project Phase 6
466 (CMIP6) experimental design and organization, Geosci. Model Dev., 9, 1937 –
467 1958. https://doi.org/10.5194/gmd-9-1937-2016, 2016.
468 Fowler, M. D., Kooperman G. J., Randerson, J. T. and Pritchard M. S.: The effect of
469 plant physiological responses to rising CO2 on global streamflow, Nat. Clim.
470 Change, 9, 873-879, https://doi.org/10.1038/s41558-019-0602-x, 2019.
471 He, J., Yang, K., Tang, W., Lu, H., Qin, J., Chen, Y., and Li, X.: The first
472 high-resolution meteorological forcing dataset for land process studies over
473 China, Sci. Data, 7, 25. https://doi.org/10.1038/s41597-020-0369-y, 2020.
474 Hempel, S., Frieler, K., Warszawski, L., and Piontek, F.: A trend-preserving bias
475 correction-the ISI-MIP approach, Earth Syst. Dyn., 4, 219-236.
476 https://doi.org/10.5194/esd-4-219-2013, 2013.
477 Hoegh-Guldberg, O., Jacob, D., Taylor, M., Bindi, M., Brown, S., Camilloni, I.,
478 Diedhiou, A., Djalante, R., Ebi, K. L., Engelbrecht, F., Guiot, J., Hijioka, Y.,
479 Mehrotra, S., Payne, A., Seneviratne, S. I., Thomas, A., Warren, R., and Zhou,
480 G.,: Impacts of 1.5 º C Global Warming on Natural and Human Systems, in:
481 Global Warming of 1.5°C. An IPCC Special Report on the impacts of global
482 warming of 1.5°C above pre-industrial levels and related global greenhouse gas
483 emission pathways, in the context of strengthening the global response to the

484 threat of climate change, sustainable development, and efforts to eradicate
485 poverty, edited by: MassonDelmotte,V., Zhai, P., Pörtner, H.-O., Roberts, D.,
486 Skea, J., Shukla, P.R., Pirani, A., Moufouma-Okia, W., Péan, C., Pidcock, R.,
487 Connors, S., Matthews, J.B.R., Chen, Y., Zhou, X., Gomis, M.I., Lonnoy, E.,
488 Maycock, T., Tignor M., and Waterfield, T.]. In Press, 186-203,
489 https://www.ipcc.ch/sr15/, 2018.
490 Ji, P., and Yuan, X.: High-resolution land surface modeling of hydrological changes
491 over the Sanjiangyuan region in the eastern Tibetan Plateau: 2. Impact of climate
492 and land cover change, J. Adv. Model. Earth. Sy., 10, 2829 – 2843.
493 https://doi.org/10.1029/2018MS001413, 2018.
494 Jia, B., Cai, X., Zhao, F., Liu, J., Chen, S., Luo, X., Xie, Z., and Xu, J.: Potential
495 future changes of terrestrial water storage based on climate projections by
496 ensemble model simulations, Adv. Water Resour., 142, 103635.
497 https://doi.org/10.1016/j.advwatres.2020.103635, 2020.
498 Jung, M., Reichstein, M., and Bondeau, A.: Towards global empirical upscaling of
499 FLUXNET eddy covariance observations: Validation of a model tree ensemble
500 approach using a biosphere model, Biogeosciences, 6, 2001–2013.
501 https://doi.org/10.5194/bg-6-2001-2009, 2009.
502 Kuang, X., and Jiao, J.: Review on climate change on the Tibetan Plateau during the
503 last half century, J. Geophys. Res. Atmos., 121, 3979 – 4007.
504 https://doi.org/10.1002/2015JD024728, 2016.

505 Li, J., Liu, D., Li, Y., Wang, S., Yang, Y., Wang, X., Guo, H., Peng, S., Ding, J., Shen,
506 M., and Wang, L.: Grassland restoration reduces water yield in the headstream
507 region of Yangtze River, Sci. Rep., 7, 2162,
508 https://doi.org/10.1038/s41598-017-02413-9, 2017.
509 Li, W., Jiang, Z., Zhang, X., Li, L. and Sun, Y.: Additional risk in extreme
510 precipitation in China from 1.5 ° C to 2.0 ° C global warming levels, Sci.
511 Bull., 63, 228. https://doi.org/10.1016/j.scib.2017.12.021, 2018.
512 Liang, L., Li, L., Liu, C., and Cuo, L.: Climate change in the Tibetan Plateau Three
513 Rivers Source Region: 1960 – 2009, Int. J. Climatol., 33, 2900-2916.
514 https://doi.org/10.1002/joc.3642, 2013.
515 Liang, X., Lettenmaier, D. P., Wood, E. F., and Burges, S. J.: A simple hydrologically
516 based model of land surface water and energy fluxes for general circulation
517 models, J. Geophys. Res., 99, 14,415-14,428. https://doi.org/10.1029/94JD00483,
518 1994.
519 Marcott, S. A., Shakun, J. D., Clark, P. U., and Mix, A. C.: A Reconstruction of
520 Regional and Global Temperature for the Past 11,300 Years, Science, 339, 1198
521 – 1201. https://doi.org/10.1126/science.1228026, 2013.
522 Martens, B., Miralles, D. G., Lievens, H., van der Schalie, R., de Jeu, R. A. M.,
523 Fernández-Prieto, D., Beck, H. E., Dorigo, W. A., and Verhoest, N. E. C.:
524 GLEAM v3: satellite-based land evaporation and root-zone soil moisture, Geosci.
525 Model Dev., 10, 1903–1925. https://doi.org/10.5194/gmd-10-1903-2017, 2017.

526 Marx, A., Kumar, R., and Thober, S.: Climate change alters low flows in Europe
527 under global warming of 1.5, 2, and 3 ° C, Hydrol. Earth. Syst. Sc., 22, 1017 –
528 1032. https://doi.org/10.5194/hess-22-1017-2018, 2018.
529 Meinshausen, M., Nicholls, Z. R. J., Lewis, J., Gidden, M. J., Vogel, E., Freund, M.,
530 Beyerle, U., Gessner, C., Nauels, A., Bauer, N., Canadell, J. G., Daniel, J. S.,
531 John, A., Krummel, P. B., Luderer, G., Meinshausen, N., Montzka, S. A., Rayner,
532 P. J., Reimann, S., Smith, S. J., van den Berg, M., Velders, G. J. M., Vollmer, M.
533 K., and Wang, R. H. J.: The shared socio-economic pathway (SSP) greenhouse
534 gas concentrations and their extensions to 2500, Geosci. Model Dev., 13, 3571 –
535 3605, https://doi.org/10.5194/gmd-13-3571-2020, 2020.
536 Meinshausen, M., Vogel, E., and Nauels, A., Lorbacher, K., Meinshausen, N.,
537 Etheridge, D. M., Fraser, P. J., Montzka, S. A., Rayner, P. J., Trudinger, C. M.,
538 Krummel, P. B., Beyerle, U., Canadell, J. G., Daniel, J. S., Enting, I. G., Law, R.
539 M., Lunder, C. R., O'Doherty, S., Prinn, R. G., Reimann, S., Rubino, M., Velders,
540 G. J. M., Vollmer, M. K., Wang, R. H. J., and Weiss, R.: Historical greenhouse
541 gas concentrations for climate modelling (CMIP6), Geosci. Model Dev., 10,
542 2057-2116. https://doi.org/10.5194/gmd-10-2057-2017, 2017.
543 Mohammed, K., Islam, A. S., Islam, G. M. T., Alfieri, L., Bala, S. K., and Khan, M. J.
544 U.: Extreme flows and water availability of the Brahmaputra River under 1.5 and
545 2 ° C global warming scenarios, Climatic Change, 145, 159-175.
546 https://doi.org/10.1007/s10584-017-2073-2, 2017.

547 Morice, C. P., Kennedy J. J., Rayner N. A., and Jones P. D.: Quantifying uncertainties
548 in global and regional temperature change using an ensemble of observational
549 estimates: The HadCRUT4 dataset, J. Geophys. Res., 117, D08101.
550 https://doi.org/10.1029/2011JD017187, 2012.
551 Oleson, K. W., Lawrence, D. M., Bonan, G. B., Drewniak, B., Huang, M., Koven, C.
552 D., Levis, S., Li, F., Riley, W. J., Subin, Z. M., Swenson, S. C., Thornton, P. E.,
553 Bozbiyik, A., Fisher, R., Heald, C. L., Kluzek, E., Lamarque, J. F., Lawrence, P.
554 J., Leung, L. R., Lipscomb, W., Muszala, S., Ricciuto, D. M., Sacks, W., Sun, Y.,
555 Tang, J., Yang, Z. L.: Technical description of version 4.5 of the Community
556 Land Model (CLM) (Rep. NCAR/TN-503 + STR, 420), 2013.
557 O'Neill, B. C., Tebaldi, C., Vuuren, D. P. V., Eyring, V., Friedlingstein, P., Hurtt, G.,
558 Knutti, R., Kriegler, E., Lamarque, J. F., Lowe, J., Meehl, G. A., Moss, R., Riahi,
559 K., and Sanderson, B. M.: The scenario model intercomparison project
560 (ScenarioMIP) for CMIP6, Geosci. Model Dev., 9, 3461-3482.
561 https://doi.org/10.5194/gmd-9-3461-2016, 2016.
562 Samaniego, L., Kumar, R., Breuer, L., Chamorro, A., Flörke, M., Pechlivanidis, I. G.,
563 Schäfer, D., Shah, H., Vetter, T., Wortmann, M., and Zeng, X.: Propagation of
564 forcing and model uncertainties on to hydrological drought characteristics in a
565 multi-model century-long experiment in large river basins, Climatic Change, 141,
566 435-449. https://doi.org/10.1007/s10584-016-1778-y, 2017.
567 Thober, T., Kumar, R., and Waders, N.: Multi-model ensemble projections of
568 European river floods and high flows at 1.5, 2, and 3 degrees global warming,

569 Environ. Res. Lett., 13, 014003. https://doi.org/10.1088/1748-9326/aa9e35,
570 2018.
571 Vicente-Serrano, S. M., Lopez-Moreno, J. I., Begueria, S., Lorenzo-Lacruz, J.,
572 Azorin-Molina, C., and Moran-Tejeda, E.: Accurate computation of a streamflow
573 drought index, J. Hydrol. Eng., 17, 318 – 332.
574 https://doi.org/10.1061/(Asce)He.1943-5584.0000433, 2012.
575 Watkins, M. M., Wiese, D. N., Yuan, D. N., Boening, C., and Landerer, F. W.:
576 Improved methods for observing Earth's time variable mass distribution with
577 GRACE using spherical cap mascons, J. Geophys. Res. Solid Earth, 120,
578 2648-2671. https://doi.org/10.1002/2014JB011547, 2015.
579 Wiltshire, A., Gornall, J., Booth, B., Dennis, E., Falloon, P., Kay, G., McNeall, D.,
580 McSweeney, C. and Betts, R.: The importance of population, climate change and
581 CO2 plant physiological forcing in determining future global water stress, Global
582 Environ. Change, 23(5), 1083-1097.
583 http://dx.doi.org/10.1016/j.gloenvcha.2013.06.005, 2013.
584 WMO.: WMO Statement on the State of the Global Climate in 2019,
585 https://library.wmo.int/doc_num.php?explnum_id=10211, 2020.
586 Xu, R., Hu, H., Tian, F., Li, C., and Khan, M. Y. A.,: Projected climate change impacts
587 on future streamflow of the Yarlung Tsangpo-Brahmaputra River, Global Planet.
588 Change, 175: 144-159. https://doi.org/10.1016/j.gloplacha.2019.01.012, 2019.
589 Yang, K., Wu, H., Qin, J., Lin, C., Tang, W., and Chen, Y.: Recent climate changes
590 over the Tibetan plateau and their impacts on energy and water cycle: A review,

591 Global Planet. Change, 112, 79 – 91.
592 https://doi.org/10.1016/j.gloplacha.2013.12.001, 2013.
593 Yang, Y., Rodericj, M. L., Zhang, S., McVicar, T. R., and Donohue, R. J.: Hydrologic
594 implications of vegetation response to elevated CO2 in climate projections, Nat.
595 Clim. Change, 9, 44-48. https://doi.org/10.1038/s41558-018-0361-0, 2019.
596 Yuan, X., Ji, P., Wang, L., Liang, X., Yang, K., Ye, A., Su, Z., and Wen, J.: High
597 resolution land surface modeling of hydrological changes over the Sanjiangyuan
598 region in the eastern Tibetan Plateau: 1. Model development and evaluation, J.
599 Adv. Model. Earth. Sy., 10, 2806 – 2828. https://doi.org/10.1029/2018MS001413,
600 2018a.
601 Yuan, X., Jiao, Y., Yang, D., and Lei, H.: Reconciling the attribution of changes in
602 streamflow extremes from a hydroclimate perspective, Water Resour. Res., 54,
603 3886 – 3895. https://doi.org/10.1029/2018WR022714, 2018b.
604 Yuan, X., Zhang, M., Wang, L., and Zhou, T.: Understanding and seasonal forecasting
605 of hydrological drought in the Anthropocene, Hydrol. Earth. Syst. Sc., 21, 5477
606 – 5492. https://doi.org/10.5194/hess-21-5477-2017, 2017.
607 Zhang Y., You Q., Chen C., and Ge J.: Impacts of climate change on streamflows
608 under RCP scenarios: A case study in Xin River Basin, China, Atmos. Res.,
609 178-179, 521-534. http://dx.doi.org/10.1016/j.atmosres.2016.04.018, 2016.
610 Zhao Q., Ding Y., Wang J., Gao H., Zhang S., Zhao C. Xu J. Han H., and Shangguan
611 D.: Projecting climate change impacts on hydrological processes on the Tibetan
612 Plateau with model calibration against the glacier inventory data and observed

streamflow, J. Hydrol., 573, 60-81. https://doi.org/10.1016/j.jhydrol.2019.03.043, 2019.

Zhu Q., Jiang H., Peng C., Liu J,, Fang X., Wei X., Liu S., and Zhou G.: Effects of future climate change, CO2 enrichment, and vegetation structure variation on hydrological processes in China, Global Planet. Change, 80-81, 123-135. https://doi.org/10.1016/j.gloplacha.2011.10.010, 2012.

Zhu, Z. C., Piao, S. L., Myneni, R. B., Huang, M. T., Zeng, Z. Z., Canadell, J. G., Ciais, P., Sitch, S., Friedlingstein, P., Arneth, A., Cao, C. X., Cheng, L., Kato, E., Koven, C., Li, Y., Lian, X., Liu, Y. W., Liu, R. G., Mao, J. F., Pan, Y. Z., Peng, S. S., Penuelas, J., Poulter, B., Pugh, T. A. M., Stocker, B. D., Viovy, N., Wang, X. H., Wang, Y. P., Xiao, Z. Q., Yang, H., Zaehle, S., and Zeng, N.: Greening of the Earth and its drivers, Nature Climate Change, 6(8), 791-+, https://doi.org/10.1038/Nclimate3004, 2016.

627

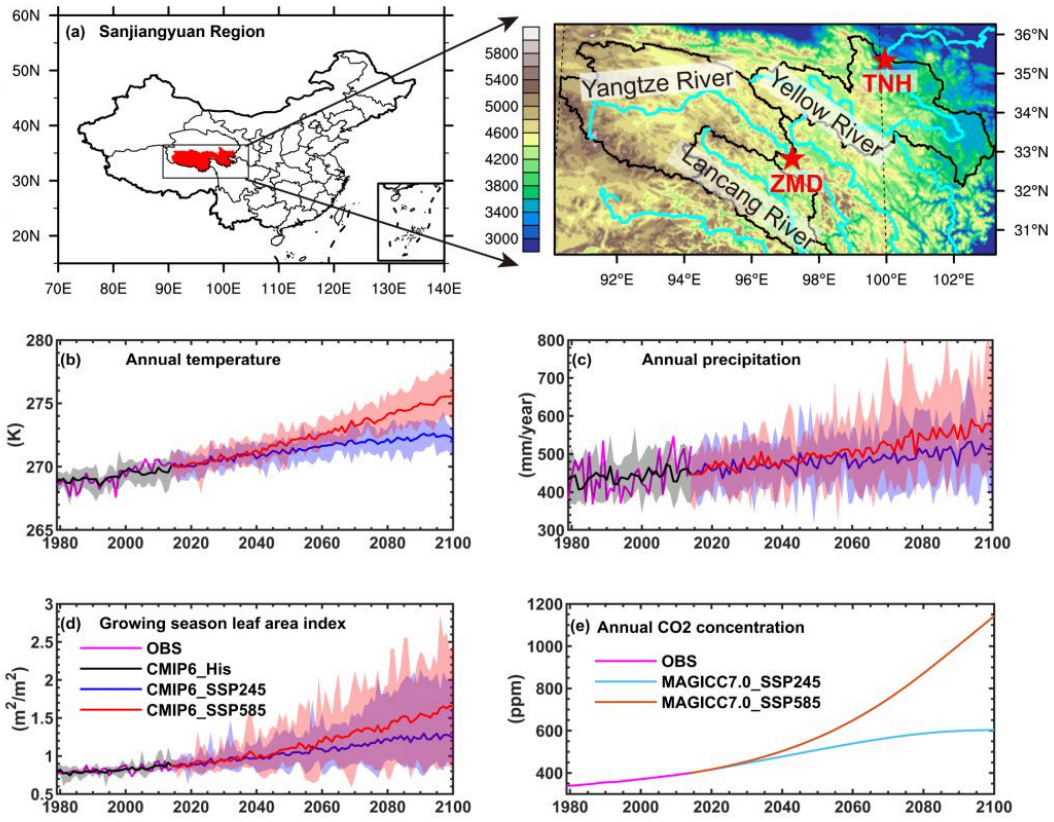

628

629 **Figure 1.** (a) The locations of the Sanjiangyuan region and streamflow gauges. (b)-(d)
630 The time series of annual temperature, precipitation, and growing season leaf area
631 index averaged over the Sanjiangyuan region during 1979-2100. (e) Observed and
632 simulated annual CO_2 concentration over the Sanjiangyuan region. Red pentagrams in
633 (a) are two streamflow stations named Tangnaihai (TNH) and Zhimenda (ZMD).
634 Black, blue and red lines in (b-d) are ensemble means of CMIP6 model simulations
635 from the historical, SSP245 and SSP585 experiments. Shadings are ranges of
636 individual ensemble members. Cyan and brown lines in (e) are future CO_2
637 concentration under SSP245 and SSP585 scenarios simulated by MAGICC7.0 model.

638

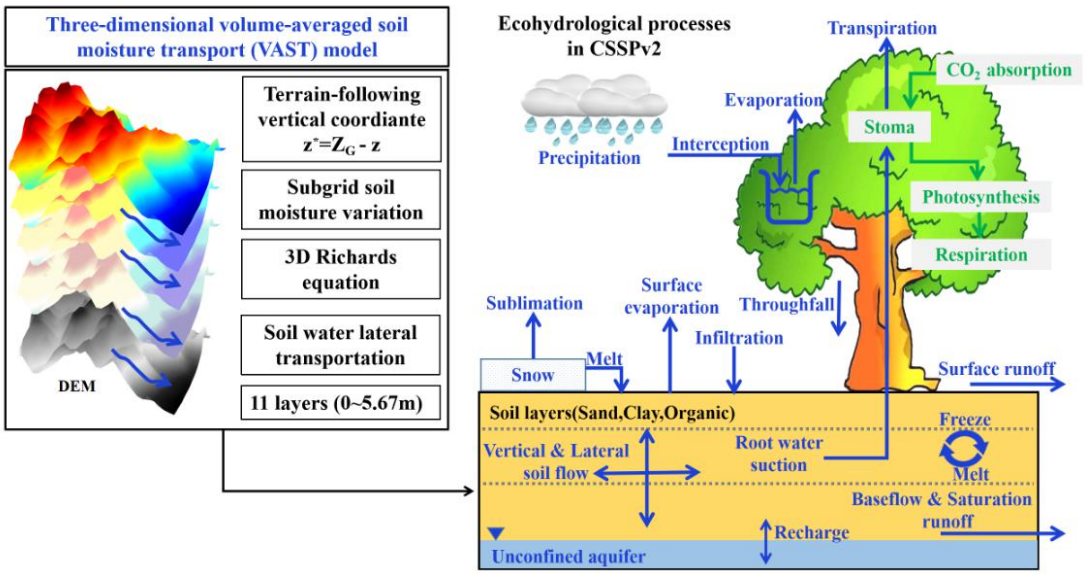

Figure 2. Main ecohydrological processes in the Conjunctive Surface-Subsurface Process version 2 (CSSPv2) land surface model.

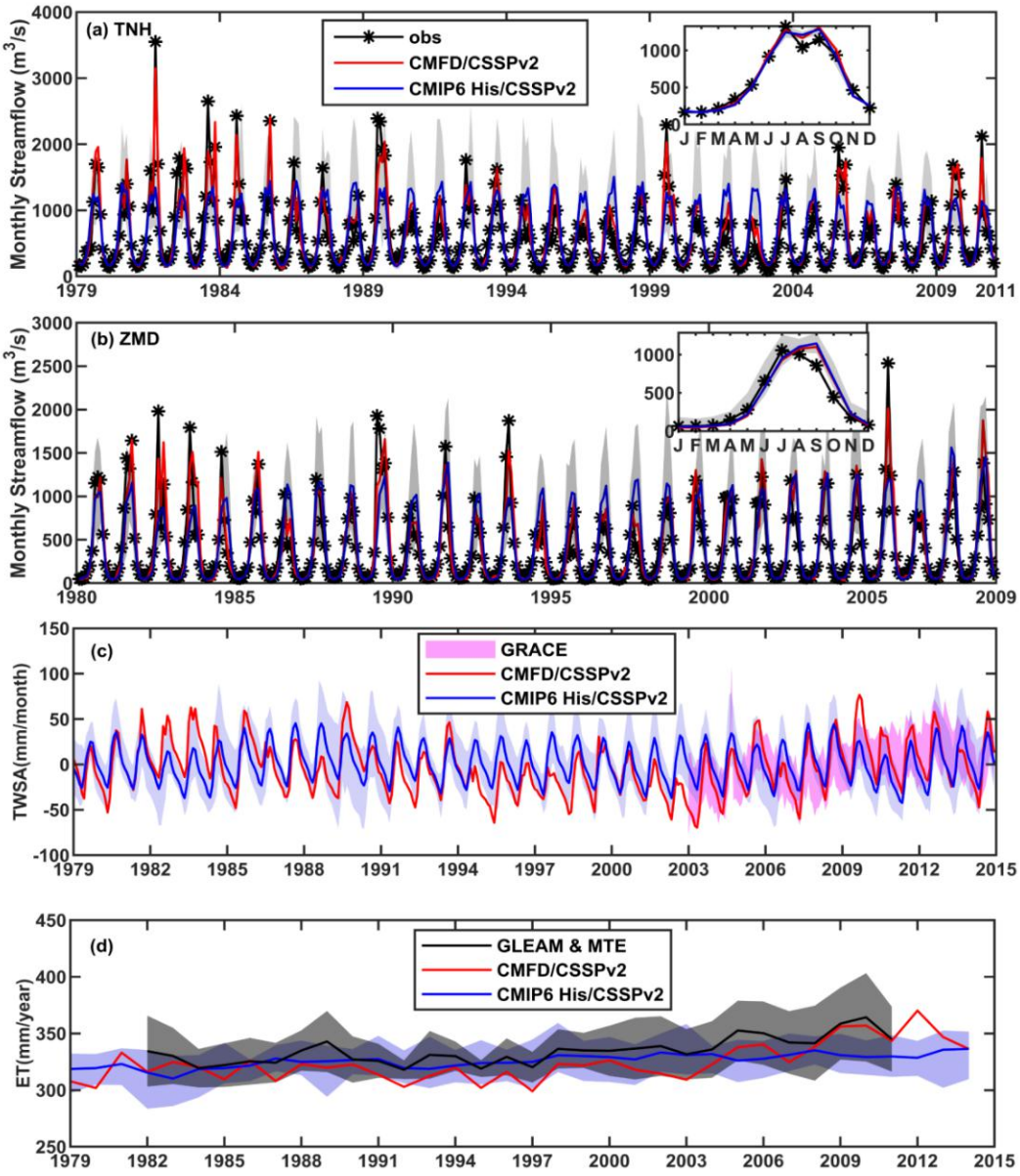

643

644 **Figure 3.** Evaluation of model simulations. (a-b) Observed and simulated monthly
645 streamflow at the Tangnaihai (TNH) and Zhimenda (ZMD) hydrological stations, with
646 the climatology shown in the upper-right corner. (c-d) Evaluation of the simulated
647 monthly terrestrial water storage anomaly (TWSA) and annual evapotranspiration (ET)
648 averaged over the Sanjiangyuan region. Red lines are CSSPv2 simulation forced by
649 observed meteorological forcing. Blue lines represent ensemble means of 11
650 CMIP6_His/CSSPv2 simulations, while gray shadings in (a-b) and blue shadings in
651 (c-d) are ranges of individual ensemble members. Pink shading in (c) is GRACE

652 satellite observations. Black line and black shading in (d) are ensemble mean and
653 ranges of GLEAM_ET and MTE_ET datasets.
654
655

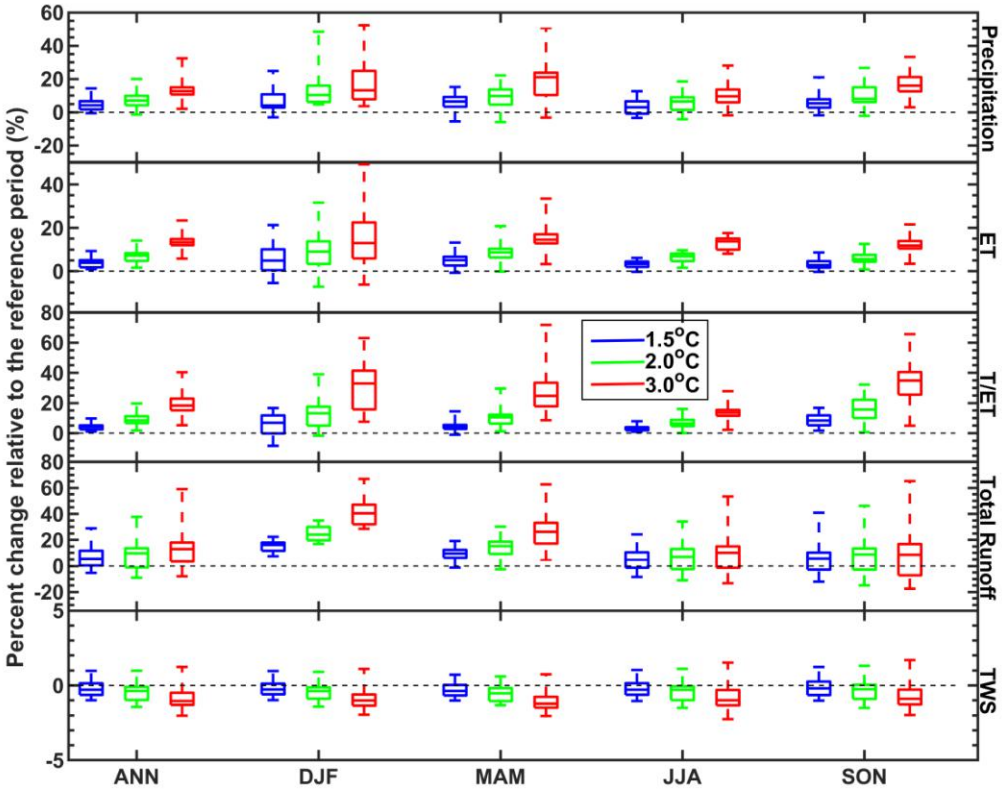

Figure 4. Box plots of relative changes of regional mean precipitation, evapotranspiration (ET), ratio of transpiration to evapotranspiration (T/ET), total runoff and terrestrial water storage (TWS) at different global warming levels. Reference period is 1985-2014, and annual (ANN) and seasonal (winter: DF, spring: MAM, summer: JJA and autumn: SON) results are all shown. Boxes show 25th to 75th ranges among 22 CMIP6_SSP/CSSPv2 simulations, while lines in the boxes are median values.

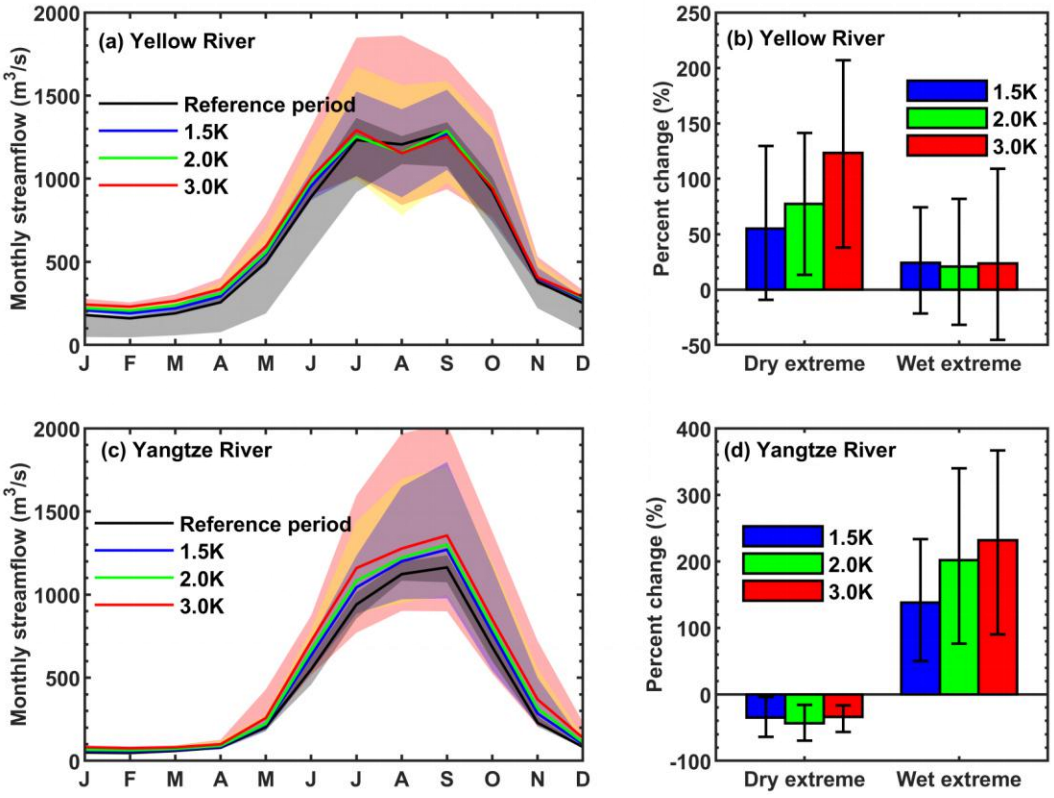

Figure 5. Changes of streamflow and its extremes at the outlets of the headwater regions of the Yellow river and the Yangtze river, i.e., Tangnaihai gauge and Zhimenda gauge. (a) Simulated monthly streamflow over the Yellow river during the reference period (1985-2014) and the periods with different global warming levels. Solid lines represent ensemble means, while shadings are ranges of individual ensemble members. (b) Percent changes in frequency of dry and wet extremes in July-September at different warming levels. Colored bars are ensemble means, while error bars are 5~95% uncertainty ranges estimated by using bootstrapping for 10,000 times. (c) and (d) are the same as (a) and (b), but for the Yangtze river.

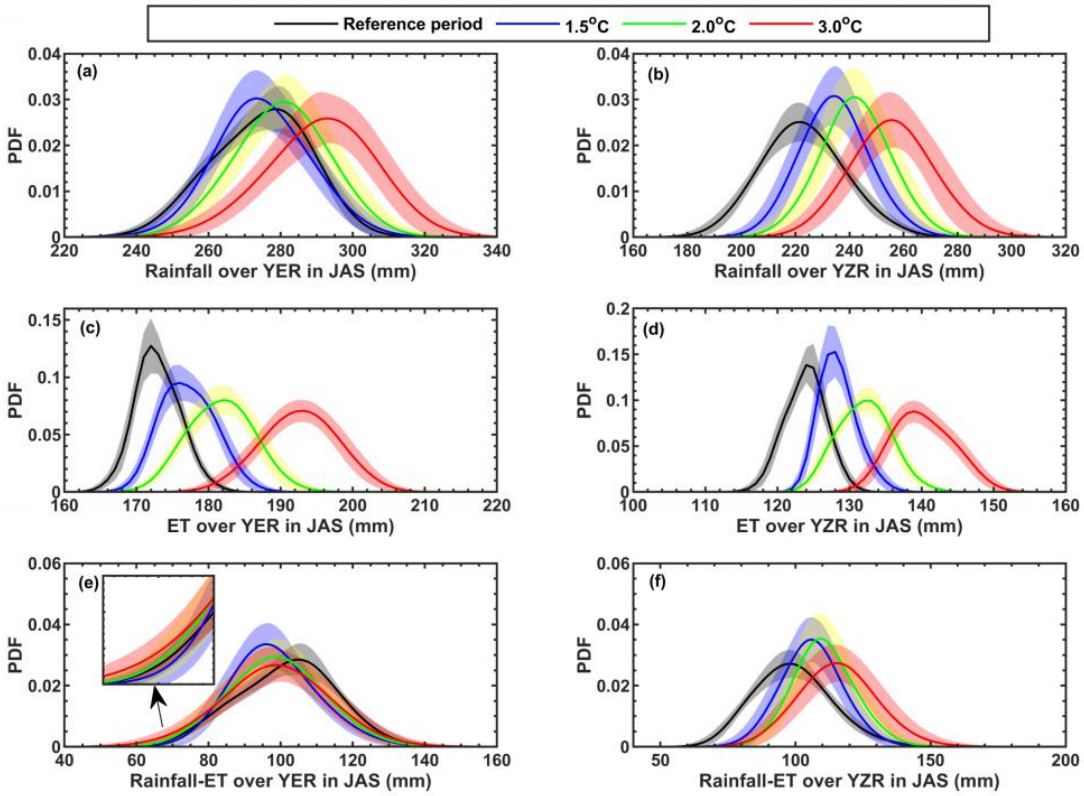

Figure 6. Probability density functions (PDFs) of regional mean rainfall, evapotranspiration (ET) and their difference over the headwater regions of Yellow river (YER) and Yangtze river (YZR) during flooding seasons (July-September) for the reference period (1985-2014) and the periods with 1.5, 2.0 and 3.0°C global warming levels. Shadings are 5~95% uncertainty ranges.

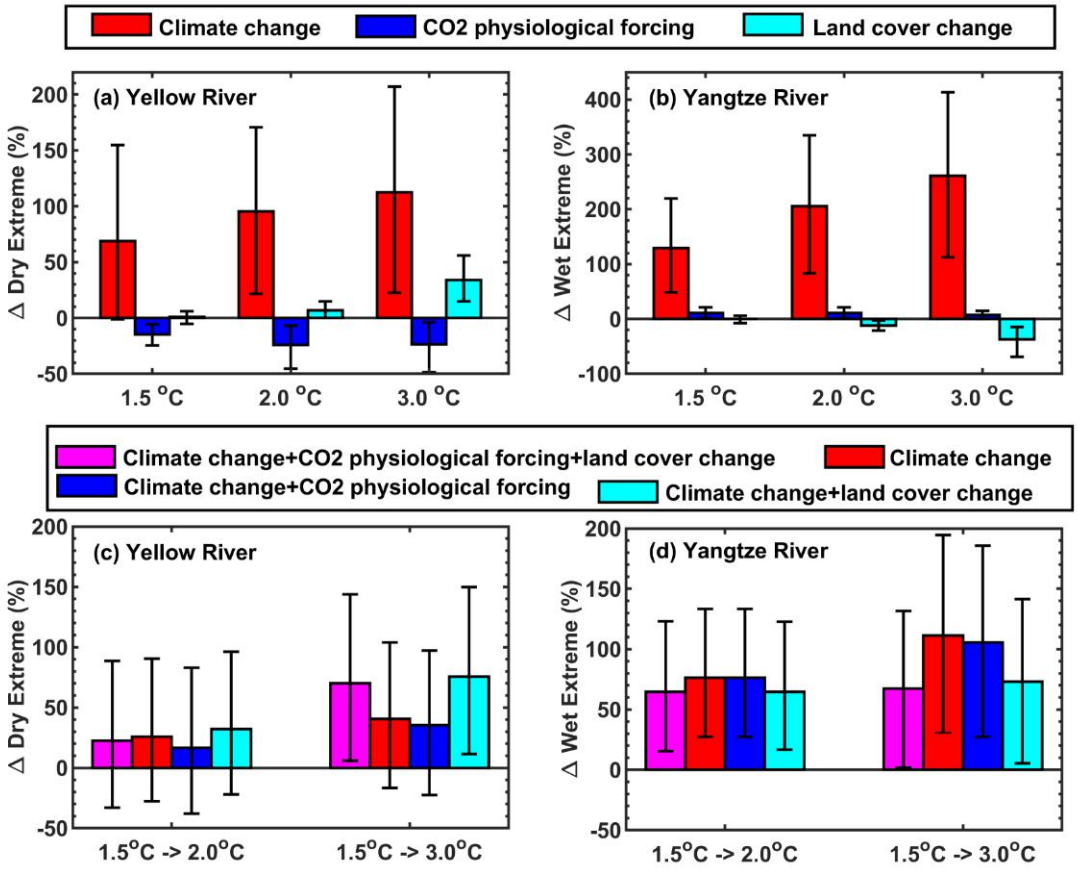

683

684 **Figure 7.** (a-b) Influences of climate change, CO_2 physiological forcing and land
685 cover change on relative changes in frequency of the dry and wet extremes in
686 July-September at different global warming levels for the headwater regions of
687 Yellow river and Yangtze river. (c-d) Changes of dry and wet extremes under
688 additional warming of 0.5°C and 1.5°C with the consideration of different factors. All
689 the changes are relative to the reference period (1985-2014). Ensemble means are
690 shown by colored bars while the 5~95% uncertainty ranges estimated by using
691 bootstrapping for 10,000 times are represented by error bars.

692

693 **Table 1.** CMIP6 simulations used in this study. His means historical simulations
694 during 1979-2014 with both anthropogenic and natural forcings, SSP245 and SSP585
695 represent two Shared Socioeconomic Pathways during 2015-2100. Note the
696 CNRM-CM6-1 and CNRM-ESM2-1 do not provide r1i1p1f1 realization, so r1i1p1f2
697 was used instead.

No.	Models	Experiments	Realization	Horizontal Resolution (Longitude × Latitude Grid Points)
1	ACCESS-ESM1-5	His/SSP245/SSP585	r1i1p1f1	192×145
2	BCC-CSM2-MR	His/SSP245/SSP585	r1i1p1f1	320×160
3	CESM2	His/SSP245/SSP585	r1i1p1f1	288×192
4	CNRM-CM6-1	His/SSP245/SSP585	r1i1p1f2	256×128
5	CNRM-ESM2-1	His/SSP245/SSP585	r1i1p1f2	256×128
6	EC-Earth3-Veg	His/SSP245/SSP585	r1i1p1f1	512×256
7	FGOALS-g3	His/SSP245/SSP585	r1i1p1f1	180×80
8	GFDL-CM4	His/SSP245/SSP585	r1i1p1f1	288×180
9	INM-CM5-0	His/SSP245/SSP585	r1i1p1f1	180×120
10	MPI-ESM1-2-HR	His/SSP245/SSP585	r1i1p1f1	384×192
11	MRI-ESM2-0	His/SSP245/SSP585	r1i1p1f1	320×160

698

699 **Table 2.** Determination of "crossing years" for the periods reaching 1.5, 2 and 3°C
700 warming levels for different GCM and SSP combinations.

Models	1.5°C warming level		2.0°C warming level		3.0°C warming level	
	SSP245	SSP585	SSP245	SSP585	SSP245	SSP585
ACCESS-ESM1-5	2024	2023	2037	2034	2070	2052
BCC-CSM2-MR	2026	2023	2043	2034	Not found	2054
CESM2	2024	2022	2037	2032	2069	2048
CNRM-CM6-1	2032	2028	2047	2039	2075	2055
CNRM-ESM2-1	2030	2026	2049	2039	2075	2058
EC-Earth3-Veg	2028	2023	2044	2035	2072	2053
FGOALS-g3	2033	2032	2063	2046	Not found	2069
GFDL-CM4	2025	2024	2038	2036	2073	2053
INM-CM5-0	2031	2027	2059	2038	Not found	2063
MPI-ESM1-2-HR	2032	2030	2055	2044	Not found	2066
MRI-ESM2-0	2024	2021	2038	2030	2074	2051

701

Table 3. Performance for CSSPv2 model simulations driven by the observed meteorological forcing (CMFD/CSSPv2) and the bias-corrected CMIP6 historical simulations (CMIP6_His/CSSPv2). The metrics include correlation coefficient (CC), root mean squared error (RMSE), and Kling-Gupta efficiency (KGE). The KGE is only used to evaluate streamflow.

Variables	Experiments	CC	RMSE	KGE
Monthly streamflow at TNH station	CMFD/CSSPv2	0.95	165 m^3/s	0.94
	CMIP6_His/CSSPv2	0.76	342 m^3/s	0.71
Monthly streamflow at ZMD station	CMFD/CSSPv2	0.93	169 m^3/s	0.91
	CMIP6_His/CSSPv2	0.82	257 m^3/s	0.81
Monthly terrestrial water storage anomaly over the Sanjiangyuan region	CMFD/CSSPv2	0.7	22 mm/month	-
	CMIP6_His/CSSPv2	0.4	24 mm/month	-
Annual evapotranspiration over the Sanjiangyuan region	CMFD/CSSPv2	0.87	14 mm/year	-
	CMIP6_His/CSSPv2	0.47	13 mm/year	-